Homogenisation of a sheared unit cell of textile composites

FEA and approximate inclusion model

Stepan V. Lomov* — Enrique Bernal — Dmitry S. Ivanov*'*** Sergey V. Kondratiev* — Ignaas Verpoest***

**Department of Metallurgy and Material Science, Katholieke Universiteit Leuven Kasteelpark Arenberg, 44, B-3001 Leuven, Belgium*

{Stepan.Lomov; Dmitry.Ivanov} @mtm.kuleuven.ac.be
{ Sergey.Kondratiev; Ignaas.Verpoest} @mtm.kuleuven.ac.be

***Facultad de Ciencias, Univesity of Zaragoza, Pza. S. Fancisco, s/n, 50009 Zaragoza, Spain*

ebernal@unizar.es

****Perm State Technical University Korolyova 6-109, 614 013 Perm, Russia*

ivmel@perm.ru

ABSTRACT. *Meso-mechanical modelling of textile composites on the "meso" (unit cell) level provides information necessary to produce homogenised properties of the composite material (with the reinforcement deformed during draping), to be used in structural analysis on the "macro" (composite part) level. The input data for the meso-calculations include geometrical model of the sheared textile and properties of the fibres and matrix. Inclusion model proceeds then to an approximate description of the reinforcement as a set of stiff inclusions, representing local orientations of the fibers, and employs the Eshelby solution and Mori-Tanaka or self-consistent homogenisation scheme to calculate the effective stiffness matrix of the composite. Finite element modelling goes through stages of (1) converting the geometrical model into a solid model; (2) meshing; (3) applying periodic boundary conditions and (4) solving a set of models necessary to calculate the homogenised stiffness matrix. All these stages present specific challenges for the case of non-orthogonal translational symmetry of the problem, which are dealt with in the paper for two types of textile reinforcements: woven and non-crimp fabrics.*

KEYWORDS: *textile composites, homogenisation.*

1. Introduction

Homogenisation of a composite material with a reinforcement deformed as the result of a forming process is an essential step in micro-macro analysis of 3D shaped textile composite parts. The main mode of deformation of the reinforcement during forming is shear, therefore the problem of homogenisation of a sheared unit cell (representative volume element) arises. The effective stiffness matrix (we confine ourselves to the elastic analysis in this paper) is assigned to the finite elements in the macro (composite part scale) calculations. The local stiffness is derived from simulations on meso (unit cell of the composite) scale, accounting for the deformations of the textile reinforcement.

Homogenisation of a textile composite is a two-stage process. The fibrous structure of the yarns or fibrous plies (in non-crimp fabrics) is homogenised to yield effective properties of the yarn or the ply (micro-problem provides input for meso-problem). Then the meso-problem is solved, yielding effective properties of the unit cell, used as input for the macro-problem. The results of micro-homogenisation are expressed in analytical formulae in function of the properties of fibres and matrix, and of the fibre volume fraction. These formulae are either empirical relations, or certain assumptions about fibre placement are used for numerical homogenisation. Two methods of the homogenisation are considered in the present paper.

The first approach is approximate and is based on Eshelby's transformation concepts. A short fibre analogy is used to describe the mechanical behaviour of curved yarn segments, combined with a Mori-Tanaka scheme to account for interaction effects. The geometrical input consists of the yarn heart-line representations and cross-sectional dimensions. Yarns are split up into segments, which are replaced by equivalent ellipsoidal inclusions using the yarn orientation and the local curvature. The homogenisation procedure is the same for orthogonal or non-orthogonal unit cell. Algorithms presented here were developed and implemented by (Huysmans *et al*., 1998).

The second approach is solving a finite element boundary value problem for a unit cell. Effective stiffness matrix is calculated as a relation between macro stress and macro strain. Such meso-level finite element modelling of textile composites recently becomes a subject of a constant stream of publications, for example (Whitcomb *et al*., 2000; Boisse *et al*., 2001; Takano *et al*., 2001; Woo *et al*., 2001; Carvelli *et al*., 2003; Zako *et al.*, 2003). However, it is surprising that non-orthogonal unit cells were not considered so far. The main challenges addressed in this paper are (1) FE model for complex sheared woven geometry, (2) FE model for non-crimp fabric (NCF) accounting for disturbances in the fibrous plies caused by stitching; (3) periodic boundary conditions for a sheared unit cell, based on theory of Whitcomb. FE models for both woven and NCF reinforcements are based on the textile simulation software WiseTex (Lomov *et al*., 2000a; Lomov *et al*., 2000b; Lomov *et al*., 2001a; Lomov *et al*., 2001b; Lomov *et al*., 2002a; Lomov *et al*., 2002b; Lomov *et al*., 2002c; Lomov *et al*., 2003). Versatility of WiseTex allows easy editing of a weave or stitching pattern and change of parameters of the reinforcement.

The inclusion model is fast and suited for processing of thousands elements of the macro-problem. An example of such a calculation could be found in (Lomov *et al*., 2004; Van den Broucke *et al*., 2004). On the contrary, FEA on the meso-level, being computationally intensive, is more suited for bench-marking. However, when non-linear behaviour and damage are considered, meso-FEA is, up to now, the only way to carry on meso-macro analysis. The methods and algorithms presented in this paper can be considered as a starting point for such an analysis.

2. Sheared unit cell of textile reinforcement

The geometrical and mechanical model of textiles, implemented in the software package *WiseTex*, provides full description of the internal geometry of a fabric: 2D and 3D woven, two- and three-axial braided, knitted, multi-axial multi-ply stitched (non-crimp fabric). The geometry in the relaxed state of the fabric is constructed using the principle of minimum energy, calculating the equilibrium of yarn interaction. For NCF the geometrical description includes fibrous plies as well as the stitching yarn. Input data include: (1) Yarn properties: geometry of the cross-section, compression, bending, frictional and tensile behaviour, fibrous content; (2) Yarn interlacing pattern; (3) Yarn spacing within the fabric repeat. Models for compression, bi-and uniaxial tension and shear are also based on energy balance and calculate internal structure of the deformed fabric, as well as load-deformation relation. The description of the internal geometry is unified both for deformed and undeformed fabrics. This section explains this description and algorithms of its conversion into FE models. The reader is referred to the papers cited above for full formulation and experimental validation of the *WiseTex* models.

2.1. *Yarns*

2.1.1. *Description of the yarns geometry in the textile modelling software*

Consider a fabric consisting of yarns only (fibrous plies in NCF are discussed below). Figure 1 illustrates the description of the spatial configuration of the yarns. The midline of a yarn is given by the spatial positions of the centres of the yarn cross-sections O: $\boldsymbol{r}(s)$, where s is coordinate along the midline, $\boldsymbol{r}$ is the radius-vector of the point O. Let $\boldsymbol{t}(s)$ be the tangent to the midline at the point O. The cross-section of the yarn, normal to $\boldsymbol{t}$, is defined by its dimensions $d_1(s)$ and $d_2(s)$ along axis $\boldsymbol{a}_1(s)$ and $\boldsymbol{a}_2(s)$. These axes are “glued” with the cross-section and rotate around $\boldsymbol{t}(s)$, if the yarn is twisted along its path (such a twist can be the result of the fabric shearing Because of this rotation the system [$\boldsymbol{a}_1\boldsymbol{a}_2\boldsymbol{t}$] may differ from the natural coordinate system along the spatial path [$\boldsymbol{nbt}$]. The shape of the cross-section can be assumed elliptical, lenticular etc. The shape type does not change along the yarn, but dimensions d_1 and d_2 can change because of different compression of the yarn in the contact zones and between them. Definition of the spatial positions of a yarn with a given cross-section shape in a unit cell consists therefore of five periodic functions: $\boldsymbol{r}$(s) (then [***nbt***] vectors can be calculated), $\boldsymbol{a_1}$(s), $\boldsymbol{a_2}$(s), $d_1(s)$, $d_2(s)$. These functions are calculated for all the yarns in the unit cell by a geometrical model.

When used in numerical calculations, all these functions are given as arrays of values for a set of points along the yarn midline.

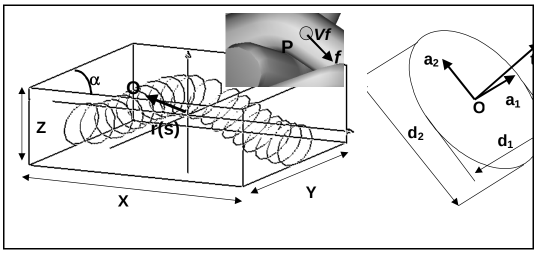

Figure 1. *Set of cross-sections defining a yarn shape in a unit cell, parameters of a cross-section and properties of fibres in the vicinity of point P*

This description fully defines the volumes of the yarns. The format is the same for orthogonal and non-orthogonal (angle α, Figure 1) unit cells. The in-plane dimensions of the unit cell *X*, *Y* are given by the repeat size of the textile structure, whereas the thickness *Z* is calculated as the difference between the maximum and minimum *z*-coordinates of the cross-sections of all the yarns in the unit cell.

The fibrous structure of the yarns, or, more generally, the fibrous structure of the unit cell is described as follows. Consider a point P and fibrous assembly in the vicinity of this point (Figure 1). The fibrous assembly can be characterised by physical and mechanical parameters of the fibres near the point (which are not necessarily the same in all points of the fabric), fibre volume fraction *Vf* and direction ***f*** of them. If the point does not lie inside a yarn, then $Vf=0$ and ***f*** is not defined. For a point inside a yarn, the fibrous properties are easily calculated, providing that the fibrous structure of the yarns in the virgin state and its dependency of local compression, bending and twisting of the yarn are given. Consider a point P. Searching the cross-sections of the yarns, the cross-sections S_i and S_{i+1}, containing between their planes the point P, are found (binary search in the unit cell volume is employed to speed up the calculations), and then by interpolation, the cross-section S, which plane contains the point P, is built. Using the dimensions of the cross-section S, for a given shape of it, point P is identified as lying inside or outside the yarn. In the former case, with the position of the point P inside the yarn known, using the model of the yarn microstructure, the parameters of fibrous assembly in the vicinity of the point P are calculated.

2.1.2. *Translation to finite element model: woven reinforcements*

The geometry of the yarn volumes can be easily transferred to a finite element description (Figure 2). A section of a yarn between neighbouring cross-sections is subdivided into four volumes (or kept intact if $d_2 / d_1 > 5$). An assembly of these volumes constitutes a solid model of the fabric. The yarn volumes are effectively meshed, using a "sweep" meshing operation: a mesh built on the first cross-section of the yarn is being "swept" through the yarn, creating a quite regular mesh. Building a mesh inside matrix is more challenging preposition and can involve manual rearrangements of the volumes built with the described procedure (see an example in section 4.2).

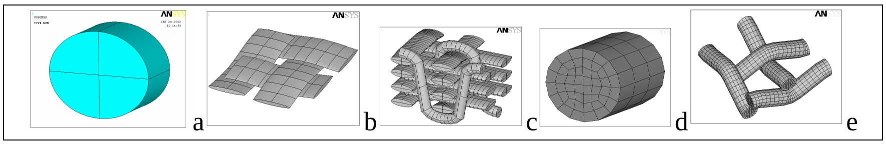

Figure 2. *Finite element models of yarns: volume between two neighbouring cross-sections, two examples of solid model of a fabric, mesh in the yarns*

For all the yarns a transversal isotropic material model is used, the properties of the impregnated yarns calculated with the formulae of (Chamis, 1989), using local fibre volume fraction and fibre orientation in the yarns (assumed constant within one segment between two neighboring cross-sections).

2.2. *Fibrous plies*

2.2.1. *Description of the plies geometry in the textile modelling software*

Multi-axial multi-ply stitched preforms (also called "non-crimp fabrics", NCF) are now a class of textile reinforcements, widely used in composites. The plies of the preform are formed as a continuous layer of parallel fibres, placed as uniformly as the technology allows (Lomov *et al*., 2002a). These plies are formed by placement of thick tows, but the tows are spread as fine as possible before placement, and they are positioned as close together as possible. As the technology allows usage of tows of a variety of thickness and width (which can be larger then the spacing of knitting needles), and as the tows can be placed with any chosen orientation, it is impossible to assure that the knitting needles would go through the plies at positions in between the tows. The needles can penetrate the spread fibre bundles, and the production parameters of the machine are set in such a way as to minimise possible fibre damage. The process of piercing of the fibrous ply by the needle and forming of the stitching (warp-knitted) loop results in a certain disturbance of the uniform placement of the fibres. These disturbances can cause resin rich regions in the composite, affecting the mechanical performance of the composite.

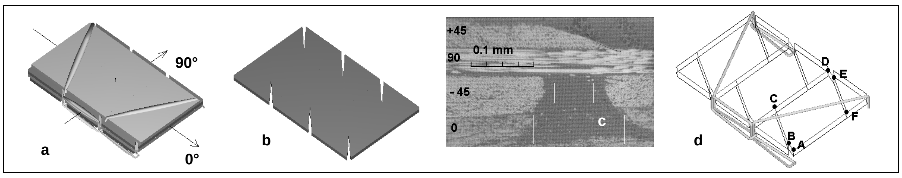

Figure 3. *Quadriaxial NCF, orientation of the fibres in the plies 0°/-45°/90°/45°, (a) Full geometrical model with stitching. Note a "channel" in the first 0° ply; (b) "cracks" in the –45° ply; (c) Channels/cracks width in cross-sections of the composite plate, thick white lines show width of the cracks as computed by the model; (d) Slab representation of a ply with -45° "cracks"*

The description of the geometry of NCF includes the geometry of the stitching yarns and geometry of the fibrous plies. The full description of the stitching yarn geometry can be found in (Lomov *et al*., 2002a). We will consider here only NCF stitched with thin non-load-carrying yarns. In this case the stitching yarn itself does not contribute to the stiffness of the composite, and therefore can be neglected in homogenising calculations. However, the stitching, even thin, interacts with the fibrous plies, which are unidirectional arrays of fibres with approximately constant thickness. The stitching causes deviations of the fibres in a ply from their uniform directions. These deviations produce fibre-free zones near stitching locations, which are regularly spaced over the ply. The fibre-free zones can be local (and called "cracks" below), or can form continuous channels in the ply (Figure 3). The local fibre volume fraction in a ply is increased and voids are created as a result of the stitching. The increased local fibre volume fraction is approximately constant in the ply.

The width and length of the "cracks" and "channels" should be measured or calculated with empirical formulae based on dimensions of the stitching yarn (Lomov *et al.* 2002a). When sheared, the fibre density in the plies increases, and the width of the "cracks" and "channels" decreases. After shear angle of 30° the width reaches its minimum. This change of the width in shear is described by empirical formulae (Loendersloot *et al.* 2003a; Loendersloot *et al.* 2003b).

The complex geometry of a fibrous ply with "cracks" and "channels" is represented in the *WiseTex* model as a set of "slabs". A slab is a volume formed by two parallel polygons. Vertices of all the slabs are stored in the counter-clockwise order (Figure 3d).

Direction of the fibres in the sheared plies is calculated by a geometrical formula

$$\tan\alpha = \tan\alpha_0 \frac{\cos\gamma}{1+\sin\gamma\tan\alpha_0} \qquad [1]$$

where α_0, α are the fibre directions before and after shearing, γ is the shear angle.

2.2.2. *Translation to finite element model: non-crimp fabrics*

In order to perform the automatic finite element mesh generation of a multi-axial multi-ply stitched (non-crimp fabric) preform, three main issues need to be addressed. First, geometrical model provided by the software package *WiseTex* must be prepared prior the mesh generation to build a good quality mesh; secondly, an automatic procedure is needed to generate a continuous model satisfying the compatibility conditions and, finally, resulting meshes on boundary surfaces must have matching node patterns in order for periodic boundary conditions to be applied in analysis. When dealing with complex 3D geometries, current state-of-the-art dictates that volumes be decomposed such that sweeping algorithms of mesh generation could be used. This technique is applied for a ply, obtaining a set of simpler areas that can be directly meshed (Figure 4a).

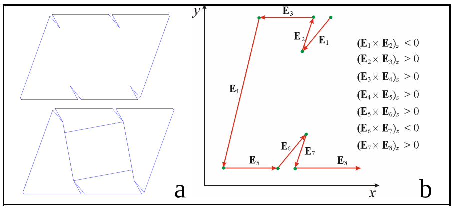

Figure 4. *Ply decomposition: Principle (a) and a reversal vertex identification (b)*

Identification of locations at which to divide the solid model is accomplished using the vector method. Given two consecutive vertex positions, $\mathbf{v}_i$ and $\mathbf{v}_{i+1}$, an edge vector between them is defined as $\mathbf{E_i} = \mathbf{v}_{i+1} - \mathbf{v}_i$. The identification algorithm calculates the cross products of successive edge vector in counter-clockwise order around the ply perimeter. A reversal vertex exists at $\mathbf{v}_k$ if the z component of the cross product $\mathbf{E}_{k-1} \times \mathbf{E}_k$ is negative. Figure 4b illustrates this process.

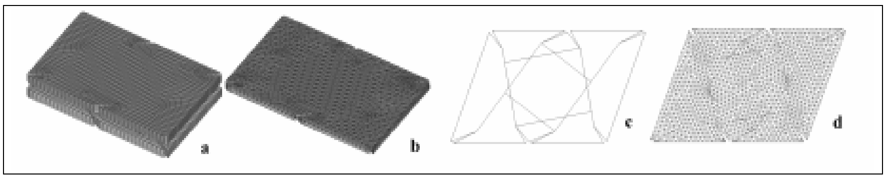

Figure 5. *Automatic meshing: (a) Hexaedral finite elements created by sweeping operation;. (b) Tetrahedral mesh built in the transition region; (c) Composite surface at the interface between plies; (d) 2D conforming mesh at the interface*

Surfaces generated at the geometry decomposition stage are then meshed using quadrilateral elements, and resulting mesh is projected (swept) through the thickness direction, thus obtaining regular hexahedral elements (Figure 5a). Meshes obtained in this way are, in general, unconnected finite element domains whose nodes do not coincide along their common boundaries. In order to preserve nodal connectivity across interface, a transition region is built by using an intermediate space to glue partitioned domains using tetrahedral elements (Figure 5b). This technique provides a useful method to satisfy the continuity and the compatibility conditions on non-conforming interfaces between consecutive plies without increasing significantly the computational cost.

Finally, matching node patterns are defined on model boundaries by translating node positions along the fabric periodicity vectors. The FE model obtained in this way is suitable for applying periodic boundary conditions according to the homogenisation scheme outlined in section 4.

3. Approximate homogenisation: method of inclusions

A detailed discussion of the inclusion model can be found in (Huysmans *et al.* 1998; Huysmans 2000), where the model was applied to warp knitted fabric composites. In the following, only the main principles are resumed.

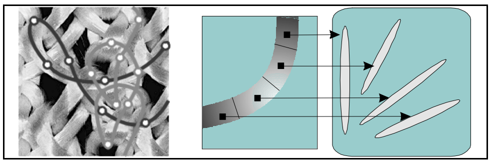

Figure 6. *Transformation of a yarn path into a set of elliptical inclusions*

Yarns in the unit cell are subdivided into a number of smaller segments (Figure 6), where each yarn segment is geometrically characterised by its total volume fraction, spatial orientation, cross-sectional aspect ratio and local curvature (all these parameters are readily provided by the geometrical model). Next, Eshelby's equivalent inclusion principle (Eshelby, 1957) is adopted to transform each heterogeneous yarn segment into homogeneity with a fictitious transformation strain distribution. Although the heterogeneous problem is reduced to a localisation problem in a homogenous medium by this transformation, the computation of the perturbed stress field still remains a complex task due to the complexity of the yarn geometry itself.

The solution makes use of a short fibre equivalent, which physically reflects the drop in the axial load carrying capability of a curved yarn with respect to an initially straight yarn. Every yarn segment is hence linked to an equivalent short fibre, possessing an identical cross-sectional shape, volume fraction and orientation as the original segment it is derived from. The length of the equivalent fibre on the other hand is related to the curvature of the original yarn. For textiles with smoothly varying curvature radii, a proportional relationship between the short fibre length and the local yarn curvature radius is the most straightforward choice and sufficiently accurate for the present purpose. The major advantage of the exploited equivalency is that the determination of the stress field in a short fibre (which can be approximated by an ellipsoid), embedded in an infinite matrix (the dilute suspension), is well known and can be obtained through Eshelby's tensor.

The interaction problem between the different reinforcing yarns is solved in the traditional way, by averaging out the image stress sampling over the different phases. If a Mori-Tanaka scheme (Mori *et al.*, 1973) is used, the stiffness tensor $\mathbf{C}^C$ of the composite is hence obtained as:

$$\mathbf{C}^C = \left[c_m \mathbf{C}^m + \left\langle c_s \mathbf{C}^s \mathbf{A}^s \right\rangle \right] \left[c_m \mathbf{I} + \left\langle c_s \mathbf{A}^s \right\rangle \right]^{-1} \qquad [2]$$

where the subscripts m and s denote the matrix and a yarn segment respectively, c_i is the volume fraction of phase i (i = m,s), and the angle brackets denote a configurational average.

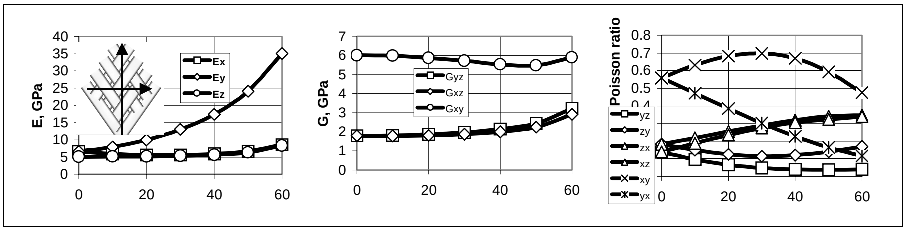

Figure 7. *Elastic properties of a sheared unit cell of a twill glass fabric as functions of shear angle, degree*

Note that the stiffness of the yarn segment $\boldsymbol{C}^s$ is a result of homogenisation on fibre level, depending on the fibre volume fraction inside the segment.

The tensor $\mathbf{A}^s$ is the localisation tensor for segment s, and is given by:

$$\mathbf{A}^s = \left[\mathbf{I} + \mathbf{S}^s \mathbf{C}^{m-1} \left(\mathbf{C}^s - \mathbf{C}^m \right) \right]^{-1} \qquad [3]$$

The Eshelby tensor $\mathbf{S}^s$ in Equation [3] depends upon the shape of the equivalent short fibre representing the yarn segment, and the properties of the matrix. If the matrix is isotropic, a valid assumption for most practical polymer matrices, the Eshelby tensor is conveniently calculated, following equations in (Eshelby, 1957). As follows from this brief description, the homogenisation procedure does not depend on the configuration of the unit cell. Figure 7 illustrates the homogenisation results for a twill fabric glass composite for different shear angles.

4. Homogenisation using FEA

With the zero-order homogenisation assumptions, formulated in Introduction, to determine the effective properties of an elastic medium, six boundary value problems for a unit cell have to be solved denoted as *(i,n), i,n=1…3*. In a problem *(i,n)* the macro strain tensor has only one non-zero component: $\langle \varepsilon^{(i,n)} \rangle = \varepsilon_{\infty}^{(i,n)}$, where $\langle ... \rangle$ is averaging over all the elements in the unit cell. The six problems to be solved correspond to *(i,n)* = (1,1); (2,2); (3,3); (1,2); (2,3); (1,3).

As the problem is linear, the value of $\langle \varepsilon^{(i,n)} \rangle$ is of no importance; we assume below $\langle \varepsilon^{(i,n)} \rangle = 1$. In this case the boundary conditions expressing continuity of stress strain field in the periodically translated unit cells are written as follows:

$$u_k^{(i,n)}(\mathbf{2}) - u_k^{(i,n)}(\mathbf{1}) = \Delta x_n \delta_{ki}; \mathbf{2}_n = \mathbf{1}_n + \Delta x_n \qquad [4]$$

where **1** and **2** are points on the unit cell boundary, corresponding to one another as prescribed by periodicity; in all the formulae the standard summation convention is used; no summation on indices in brackets. Effective stiffness C^{eff} of the structure are then calculated as: $C_{glin}^{eff} = \langle C_{glpq} u_{p,q}^{(i,n)} \rangle$, where C is stiffness of an element.

4.1. ***Boundary conditions for homogenisation of a sheared unit cell of a square plane weave***

Apart from the translation of the unit cell as a whole, it can have other properties of symmetry, which would allow reducing the FE model to a model of ½, ¼ etc part of the unit cell, hence reducing the computational complexity of it. (Whitcomb *et al.*, 2000) proposed a transformation technique for that purpose. However, only orthogonal woven unit cells are studied by Whitcomb. As non-orthogonal woven unit cells have another symmetry type (non-orthotropic), there is a need to adapt the transformation technique to this case.

Consider a unit cell of a sheared square plain weave reinforcement (Figure 8), which can be divided in four identical quadrants. The whole unit cell can be reproduced by rotation, mirroring and translation of the quarter. Here an outline of the derivation of the boundary conditions is given.

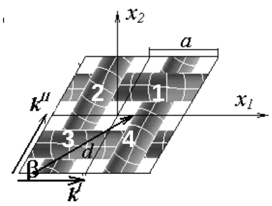

Figure 8. *Vectors **d, k^I**, **k^{II}** for plain weave reinforcement; numbers of the quadrants of the unit cell*

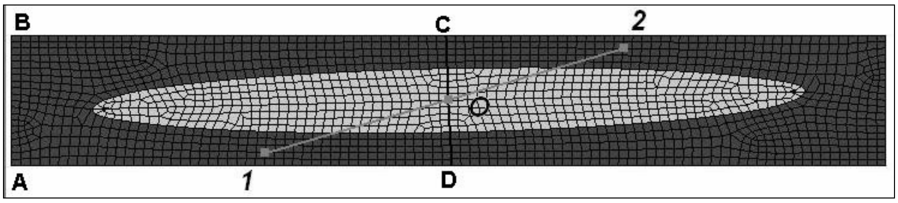

Figure 9. *Corresponding points and mesh on the face of a quarter of the sheared unit cell*

Define vectors oriented in the directions of warp and weft yarns $\mathbf{k}^{\mathbf{I}}$, $\mathbf{k}^{\mathbf{II}}$ are given by (β is the unit cell angle, see Figure 8)

$$\mathbf{k}^{\mathbf{I}} = (a,0,0), \mathbf{k}^{\mathbf{II}} = (c-a,b,0); c = a\left(1+\cos\beta\right), b = a\sin\beta$$

We also will use vector $\mathbf{d} = \left(\mathbf{k}^{\mathbf{I}} + \mathbf{k}^{\mathbf{II}}\right)/2 = \left(c,b,0\right)$. Following (Whitcomb *et al.*, 2000), we introduce transformations of coordinates, which leave the unit cell intact, and also satisfy the periodic conditions (4):

1. *Rotation around the x_3 axis by π.* The transformation establishes a correspondence between the first – third and second – fourth quadrants of the unit cell.

2. *Mirroring relative to the plane x_3=0 and translation by **k^I** or **k^{II}**.* The transformation establishes a correspondence between the first – second and third – fourth quadrants of the unit cell.

The directional cosines matrices of these two transformations are:

$$\alpha' = \begin{pmatrix} -1 & 0 & 0 \\ 0 & -1 & 0 \\ 0 & 0 & 1 \end{pmatrix}, \alpha'' = \begin{pmatrix} 1 & 0 & 0 \\ 0 & 1 & 0 \\ 0 & 0 & -1 \end{pmatrix}$$

The two transformations together give correspondence of the first quadrant of the unit cell will all others. Applying the technique of (Whitcomb *et al*., 2000), and using the notation of γ, introduced in his paper, we obtain a set of boundary conditions, summarised in Table 1. Note that the corresponding points are *on the same face* of the quarter of the unit cell. This is because a complex set of transformation was used. Equation [4] for the full unit cell, accounting only for its translation symmetry as a whole, connects points on the opposite faces. Boundary conditions of Table 1 are generalisation of equations (Whitcomb *et al*., 2000) for an orthogonal unit cell.

Table 1. *Boundary conditions for the quarter of plain weave composite*

Face	*Corresponding points* (ξ_0,η)	*Boundary condition* $u_j^{(i,n)}(\mathbf{1})+u_j^{(i,n)}(\mathbf{2})=\delta_{ij}\cdot\ldots$
$x_2 \equiv b$	$(c-x_1,b,x_3)\to(c-x_1-a,b,-x_3)$	$\ldots\cdot\left(k_n^{II}+\gamma\alpha''_{np}d_p\right)$
$x_2 \equiv 0$	$(x_1,0,x_3)\to(a-x_1,0,-x_3)$	$\ldots\cdot\left(k_n^{II}+\gamma\alpha'_{np}d_p\right)$
$x_1 = x_2\cot\beta +$	$(x_2\cos\beta+a,x_2,x_3)\to$ $(c-x_2\cos\beta,b-x_2,-x_3)$	$\ldots\cdot\left(k_n^{I}+\gamma\alpha''_{np}d_p\right)$
$x_1 = x_2\cot\beta$	$(x_2\cos\beta,x_2,x_3)\to$ $(c-x_2\cos\beta-a,b-x_2,-x_3)$	$\ldots\cdot\left(k_n^{I}+\gamma\alpha'_{np}d_p\right)$
$\gamma=-1$ if *(i,n)* = (1,3) or (2,3); $\gamma=1$ if *(i,n)*= (1,1), (2,2), (3,3) or (1,2)		

Note that the boundary conditions for the unit cell quarter restrict not a difference between the nodal displacement but a sum of the them. For the central points of the faces (point O, Figure 9) the corresponding points **1** and **2** are infinitely close, and conditions of Table 1 give a value for the displacement of the central point, preventing movement of the unit cell as rigid body.

4.2. *Homogenisation of a sheared unit cell of woven composite*

This section describes FE modelling of a woven glass composite, with the parameters shown in Figure 10 and Table 2.

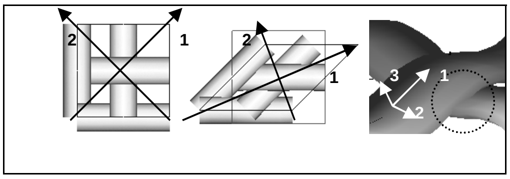

Figure 10. *Unsheared and 45° sheared plain woven fabric; (interpenetration is circled)*

Table 2. *Parameters of a woven glass/epoxy composite*

Fibres	**Glass**	**Yarns (before/after shearing)**	
Diameter, μm	21	Linear density, tex	610
Young modulus, GPa	72	Number of fibres	700
Poisson ratio	0.23	Thickness, mm	0.26/0.28
Matrix	**Epoxy**	Width, mm	1.65/1.61
Young modulus, GPa	3.0	Vf, %	75.0/73.4
Poisson ratio	0.40	**Impregnated yarns**	
Fabric	**plain weave**	E_{11}, GPa	54.7/49.1
Ends count, yarns/cm	3.6	$E_{22}= E_{33}$, GPa	17.6/13.8
Picks count, yarns/cm	3.6	ν_{12}	0.27/0.37
Thickness, mm	0.496/0.575	G_{23}, GPa	6.46/5.03
Vf, %, before/after shearing	35.0/46.4	$G_{12}= G_{13}$, GPa	6.46/5.03
		$\nu_{23}=\nu_{13}$	0.36/0.29

4.2.1. *Solid model*

A geometrical model built in *WiseTex* software was transferred to a FE package ANSYS as explained in section 2.1.2. Note that after shearing the dimensions of the yarns change: they undergo lateral compression and a bit swell in the width. Accordingly the properties of the impregnated yarns change slightly. The thickness of the fabric increases as the result of change of the yarns shape. Fibre volume fraction in the composite increases considerably because of the overall reduction of the surface of the sheared fabric. Note also twisting of the yarns as the result of shearing (Lomov *et al.*, 2002b), which can be clearly seen in Figure 9.

The unit cell of the fabric has been automatically transformed into a symmetrical configuration (compare Figure 8 and Figure 10), and a quarter of it was cut out. The FE model was built on this quadrant of the unit cell. The geometrical model of the sheared fabric has some interpenetration of the yarn volumes (Figure 10). This has been taken rid of manually. Finally, a thin layer of resin (thickness equal to 0.1 of the yarn thickness) was added on the top and the bottom of the quadrant to allow meshing.

4.2.2. *Meshing and boundary conditions*

Automatic meshing by the ANSYS meshing engine does not generate symmetrical meshes on the faces of the quadrant, as it is needed for setting of the boundary conditions of Table 1 (cf. Figure 9). The symmetrical mesh was build as follows. Shell elements were built on the faces of the quadrant. On half of the face (ABCOD in Figure 9) the mesh was constructed automatically. Then a cylindrical coordinate system was introduced with the centre in the point O and *z*-axis normal to the plane of the face. The surface mesh for the other half of the face was copied by rotating a mesh on π around the *z*-axis. After the surface mesh was ready on four faces, the volume of the quadrant was meshed by tetrahedral elements. Surface mesh and volume mesh are stitched to each other at the surface nodes. Shell elements at the surface were removed consequently.

In-plane boundary conditions for each *(i,n)* problem of the homogenisation calculations were applied as shown in Table 1. They correspond to the periodic conditions equation (4) for the applied strain $\left\langle \varepsilon^{(i,n)} \right\rangle = 1$. Horizontal faces of the quadrant were fixed: $u_z = 0$ on these faces. This corresponds to an "anti-phase" arrangements of the layers in a laminate. Results of (Zako *et al.*, 2003) show that the choice of the laminate arrangement ("phase" = periodic in *z*, "anti-phase" or nested) does not affect significantly the homogenised properties.

4.2.3. *Material properties*

Epoxy matrix was modelled as elastic material, yarns are orthotropic with properties shown in Table 2. Axis*1*should go along the yarn middle-line, axes *2* and 3 are orthogonal to it, as explained in section 2.1.2. However, because of manual transformation of the yarns volume (in the case of penetrating yarns, see above), automatic assigning of the orthotropic yarn properties was not possible, and they were assigned manually with the following approximation: axis *1* had an average direction of the yarn middle-line between the intersections (Figure 10). Because of a quite shallow crimp of the yarns (crimp coefficient 0.4%) this simplification should not affect much the homogenised properties.

4.2.4. *Results*

In-plane stiffness components of the composite (Table 3) are expressed in the bias coordinate system *(12)*, corresponding to the directions of orthotropy, as shown in Figure 10. Figure 11 illustrates strain distribution in different loading cases.

Table 3. *In-plane stiffness of the glass/epoxy woven composite, calculated with FE modelling and inclusion model, GPa*

Shear angle,°		C_{1111}	C_{1122}	C_{1112}	C_{2211}	C_{2222}	C_{2212}	C_{1211}	C_{1222}	C_{1212}
0	FE	13.8	9.2	-0.01	9.2	13.8	-0.01	0	-0.01	6.4
	Incl.	14.0	9.2	0.05	9.2	14.0	0.05	0.05	0.05	6.1
45	FE	25.5	7.8	0.03	7.8	11.5	0.01	0.03	0.01	5.3
	Incl.	27.6	8.82	0	8.8	12.6	0	0	0	5.9

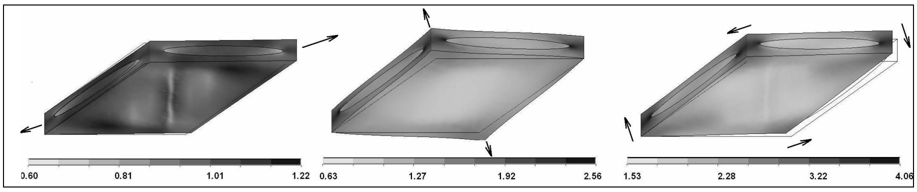

Figure 11. *Strain fields in the composite. Loading cases correspond to the component of the strain displayed (* $\varepsilon_{11}, \varepsilon_{22}, \varepsilon_{12}$ *). Applied strain value is 1*

The results reveal expectable trends: (1) stiffness in the direction *1* (direction of shear) is increased, as fibers are reoriented in this direction and fibre volume fraction of the composite increases with shear; (2) stiffness in the direction *2* decreases as fibres deviate from this direction, but not much, as this effect is compensated by the increase of the fibre volume fraction; (3) the same can be said about the shear components of stiffness.

The composite is orthotropic in coordinates *(12)*, as the components C_{1112}, C_{2212}, C_{1222} are small (inside the expected error margin of the models). This is explained by a shallow crimp of the yarns, which does not introduce pronounced asymmetry in averaged stress-strain state (mid-plane of the fabric is not a plane of symmetry).

The composite stiffness was also calculated with the inclusion model (section 3.1), using exactly the same geometrical configuration (build with *WiseTex* and thin matrix layer added on top and bottom of the unit cell). The values calculated with inclusion model are fairly close to the FE results.

4.3. *Homogenisation of a sheared unit cell of non-crimp fabric-based composite*

This section contains results on homogenization of a biaxial (±45º) carbon/epoxy laminate (Figure 12 and Table 4). The geometrical model built in WiseTex software was automatically transferred to the ANSYS finite element package using the algorithm explained in section 2.2. As the result of shearing the width of the "cracks" decrease and the volume fraction in the plies increase due to the overall reduction of the surface of the sheared fabric. Prescribed displacements accounting for periodicity of the sheared unit cell, are applied to obtain the in-plane components of the fourth-order tensor **C**. Unlike the procedure outlined in the previous section dealing with homogenisation of a plane woven section, no model reduction is to be performed in this case. In-plane stiffness components of the composite is expressed in the coordinate system (*xy*), corresponding to the directions of orthotropy (Figure 12). The results are shown in Table 5 and Figure 13. The homogenised stiffness results are quite close for the predictions of Classical Laminate Theory, as it could be expected (Truong Chi *et al.*, 2001), and to experimental data (Table 6). Strain fields reveal strain concentration on the stitching loci, in correspondence with the experimentally observed distribution of the initial damage (Vettori *et al.*, 2004).

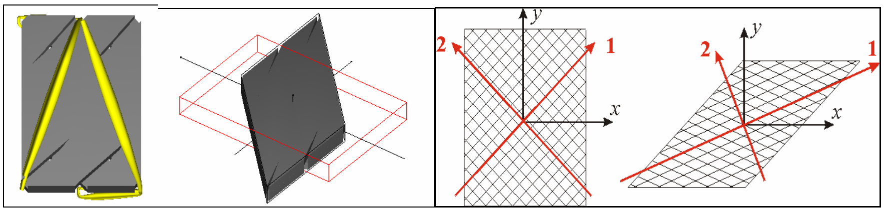

Figure 12. *Unsheared and 45° sheared NCF (left);Coordinate systems (right)*

Table 4. *Summary of properties*

Fibres	**Carbon**	**Matrix**	**Epoxy**
Diameter, µm	6.9	Young module, GPa	3.0
Young modulus, GPa, longitudinal/transversal	230/20	Poisson ratio	0.40
Poisson ratio	0.27	**Ply mech. properties (before/after shearing)**	
Fabric	**NCF**	E_{11}, GPa	64.3/89.67
Reinf. angle (before)	+45º/-45º	$E_{22} = E_{33}$, GPa	5.4/6.3
Reinf. angle (after)	+67.5º/-22.5º	$\nu_{12} = \nu_{13}$	0.36/0.35
Ply thickness, mm	0.20	$G_{12} = G_{13}$, GPa	2.09/2.55
Vf, %, before/after shearing	22.8/32.2	G_{23}, GPa	1.94/2.29
		ν_{23}	0.39/0.38

Table 5. *In-plane stiffness of the biaxial (± 45º) carbon-carbon NCF*

Shear angle,º	C.S	C_{1111}	C_{2222}	C_{3333}	C_{2211}	C_{2233}	C_{1133}	C_{1212}	C_{1313}	C_{2323}
0	*xy*	18.57	18.57	5.32	15.05	2.41	2.41	14.05	1.67	1.67
45	*xy*	58.63	7.77	5.98	11.60	2.41	2.79	10.78	1.83	2.01

Table 6. *Experimenal and computed engineering constants of the biaxial (± 45º) carbon-carbon NCF*

Shear angle,º		E_x, GPa	E_y, GPa	ν_{xy}	ν_{yx}
0	experiment	6.6±0.3	6.6±0.3	0.70±0.1	0.70±0.1
	calculated	6.3	6.3	0.78	0.78
45	experiment	34.2±6.7	5.3±0.1	1.22±0.1	0.15±0.1
	calculated	41.2	4.9	1.54	0.18

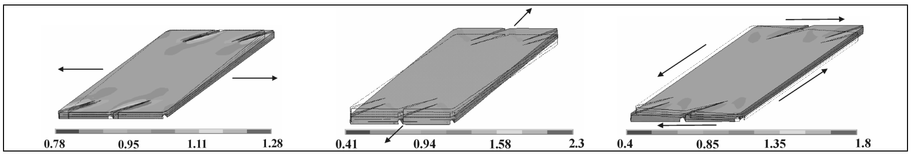

Figure 13. *Strain fields in the composite. Loading cases correspond to the components of the strain displayed ($\varepsilon_{xx}, \varepsilon_{yy}, \varepsilon_{xy}$). Applied strain values are 1*

5. Conclusions

1. Homogenisation of a sheared unit cell of textile composites is a necessary step in micro-macro analysis of composite part. Two approaches – approximate inclusion model and meso-level FE analysis – both are based on a geometrical model of deformed textile, implemented in *WiseTex* software package, which covers wide range of textile structures, including woven and non-crimp fabrics.

2. Good integration in the chain of micro-macro mechanical modelling of 3D shaped composite part (*QuikForm – WiseTex – TexComp* – SYSPLY) has been demonstrated and proven to represent a reality with a reasonable accuracy in the elastic deformation region.

3. For woven fabrics with square geometry the FE model of the sheared unit cell can be reduced to a quarter of the unit cell using the formulated boundary conditions.

Acknowledgments

The work reported here has been carried out in the scope of the projects TECABS (European Commission), “Concurrent multi-scale design/engineering of textile composites” (K.U.Leuven) and “Predictive tools for permeability, mechanical and electro-magnetic properties of fibrous assemblies” (IWT, Flanders). PhD research of DI is supported by an “East-European” grant of K.U.Leuven. EB worked in K.U.Leuven as a Marie Curie PhD Fellow of European Commission (HPMT-CT-2000-00030). Authors are grateful to Dr. S.G.Ivanov (Perm State Technical University, Russia) for his input to development of periodic boundary conditions (section 4.1).

6. References

Boisse P., Buet K., Gasser A., Launay J., “Meso/macro-mechanical behaviour of textile reinforcements for thin composites”, *Composites Science and Technology*, Vol. 61, 2001, pp. 395-401.

Carvelli V., Poggi C., “A numerical approach for the failure analysis of textile composites”, *Proceedings ICCM-14*, San Diego**,** 2003, CD edition.

Chamis C. C., “Mechanics of composite materials: Past, present and future”, *Journal of Composites Technology and Research*, Vol. 11, No. 1, 1989, pp. 3-14.

Eshelby J. D., “The determination of the elastic field of an ellipsoidal inclusion and related problems”, *Proceedings of Royal Society*, Vol. A-241, 1957, pp. 376-396.

Huysmans G., Verpoest I., Van Houtte P., “A poly-inclusion approach for the elastic modelling of knitted fabric composites”, *Acta Materials*, Vol. 46, No. 9, 1998, pp. 3003-3013.

Huysmans G., Unified micromechanical models for textile composites, PhD, Department MTM, K.U. Leuven, 2000.

Loendersloot R., Lomov S. V., Akkerman R., Verpoest I., “Architecture and permeability of sheared carbon fibre non-crimp fabrics”, *Proceedings of the 24th International SAMPE Europe Conference*, Ed.K. Drechsler, Paris**,** 2003a, pp. 141-148.

Loendersloot R., Thije R. H. W. t., Lomov S. V., Akkerman R., Verpoest I., “Geometry, Compressibility and Porosity of Sheared Non-Crimp Fabrics”, *Proceedings of the 14th SiComp Conference*, 2003b, CD edition.

Lomov S. V., Gusakov A. V., Huysmans G., Prodromou A., Verpoest I. “Textile geometry preprocessor for meso-mechanical models of woven composites”, *Composites Science and Technology*, Vol. 60, 2000a, pp. 2083-2095.

Lomov S. V., Verpoest I., “Compression of woven reinforcements: a mathematical model”, *Journal of Reinforced Plastics and Composites*, Vol. 19, No. 16, 2000b, pp. 1329-1350.

Lomov S. V., Huysmans G., Luo Y., Parnas R., Prodromou A., Verpoest I., Phelan F. R. "Textile Composites Models: Integrating Strategies", *Composites,* part A, Vol. 32**,** No. 10, 2001a, pp. 1379-1394.

Lomov S. V., Huysmans G., Verpoest I., "Hierarchy of textile structures and architecture of fabric geometric models", *Textile Research Journal*, Vol. 71**,** No. 6, 2001b, pp. 534-543.

Lomov S. V., Belov E. B., Bischoff T., Ghosh S. B., Truong Chi T., Verpoest I., "Carbon composites based on multiaxial multiply stitched preforms, Part 1: Geometry of the preform", *Composites part A*, Vol. 33, No. 9, 2002a, pp. 1171-1183.

Lomov S. V., Nakai A., Parnas R. S., Bandyopadhyay Ghosh S., Verpoest I., "Experimental and theoretical characterisation of the geometry of flat two- and three-axial braids", *Composite forming simulation*, *Textile Research Journal*, Vol. 72, No. 8, 2002b, pp. 706-712.

Lomov S. V., Verpoest I., Peeters T., Roose D., Zako M. "Nesting in textile laminates: Geometrical modelling of the laminate", *Composites Science and Technology*, Vol. 63**,** No. 7, 2002c, pp. 993-1007.

Lomov S. V., Truong Chi T., Verpoest I., Peeters T., Roose V., Boisse P., Gasser A., "Mathematical modelling of internal geometry and deformability of woven preforms", *International Journal of Forming Processes*, Vol. 6, No. 3-4, 2003, pp. 413-442.

Lomov S. V., Van den Broucke B., Tumer F., Verpoest I., De Luka P., Dufort L. "Micro-macro structural analysis of textile composite parts", *Proceedings ECCM-11*, Rodos, 2004, p. CD Edition.

Mori T., Tanaka K., "Average stress in matrix and average elastic energy of materials with misfitting inclusions", *Acta Metall.Mater.*, Vol. 21, 1973, pp. 571-574.

Takano N., Ohnishi Y., Zako M., Nishiyabu K., "Microstructure-based deep-drawning simulation of knitted fabric reinforced thermoplastics by homogenisation theory", *International Journal of Solids and Structures*, Vol. 38, 2001, pp. 6333-6356.

Truong Chi T., Lomov S. V., Verpoest I. "The mechanical properties of multiaxial multiply carbon fabric reinforced Epoxy composites", *Proceedings of the 10th European Conference on Composite Materials (ECCM-10),* Ed.H. Sol and J. Degrieck. Brugge**,** 2001, p.CD edition.

Van den Broucke B., Tumer F., Lomov S. V., Verpoest I., De Luca P., Dufort L. "Micro-macro structural analysis of textile composite parts: Case study", *Proceedings of the 25th International SAMPE Europe Conference,* March 30th - April 1st., Paris**,** 2004, pp. 194-199.

Vettori M., Truong Chi T., Lomov S. V., Verpoest I. "Progressive damage characterization of stitched, biaxial, multi-ply carbon fabrics composites", *Proceedings ECCM-11*, Rodos, 2004, p. CD edition.

Whitcomb J., Chapman C. D., Tang X., "Derivation of boundary conditions for micromechanics analyses of plain and satin woven composites", *Journal of Composite Materials*, Vol. 34, No. 9, 2000, pp. 724-747.

Woo K., Suh Y. W., "Low degree of homogenity due to phase shift for woven composites", *Journal of Composites Technology & Research* Vol. 23, No. 4, 2001, pp. 239-246.

Zako M., Uetsuji Y., Kurashiki T. "Finite element analysis of damaged woven fabric composite materials", *Composites Science and Technology*, Vol. 63, 2003, pp. 507-516.